Broadly tunable mid-infrared femtosecond pulses directly generated by an optical parametric amplifier

Research Article Vol. 4, No. 11 / 15 Nov 2021 / OSA Continuum 2837

Broadly tunable mid-infrared femtosecond pulses directly generated by an optical parametric amplifier

ANDREA VILLA,[1] AARON M. ROSS,[1] RICCARDO GOTTI,[1,2] MARCO LAMPERTI,[1,2] FRANCESCO SCOTOGNELLA,[1,2] GIULIO CERULLO,[1,2] AND MARCO MARANGONI[1,2,*]

[1]*Dipartimento di Fisica, Politecnico di Milano, Piazza Leonardo da Vinci 32, 20133 Milano, Italy*
[2]*Istituto di Fotonica e Nanotecnologie, CNR, Piazza Leonardo da Vinci 32, 20133 Milano, Italy*
[*]*marco.marangoni@polimi.it*

Abstract: We introduce an optical parametric amplifier, pumped by an amplified femtosecond Yb:KGW laser, which directly generates broadly tunable mid-infrared (MIR) pulses, covering the whole vibrational spectrum from 3 to 10 µm. The avoidance of the traditional difference-frequency generation stage to access the MIR range simplifies the setup while enabling high conversion efficiencies. The two-stage design employs in the second stage either periodically poled lithium niobate, optimized for the CH/OH stretching region (3-5 µm) or $LiGaS_2$, which allows extending the tunability to the fingerprint region (up to 10 µm). We anticipate applications of this versatile source to ultrafast vibrational spectroscopy and infrared microscopy.

1. Introduction

A large variety of near-infrared laser sources, both with and without regenerative amplification, have been exploited in recent years in combination with nonlinear optical processes for the generation of mid-infrared (MIR) light pulses, prioritizing, depending on the application, the pulse energy [1,2], the phase coherence needed for frequency comb applications [3,4], the pulse duration [5], the compactness and the conversion efficiency [6], the combination power-spectral coverage [7,8] or power-energy [9]. We pay here specific attention to nonlinear femtosecond laser sources with average power of few tens of mWs and repetition rate around 100 kHz, which are adequate parameters for ultrafast spectroscopy applications, such as transient vibrational spectroscopy [10], 2DIR spectroscopy [11] and the study of inter-subband transitions [12] and phonon-driven structural dynamics [13] in solids. Typical vibrational transitions of interest are in the 1000-1700 cm^{-1} frequency range ($\lambda = 5.8$-10 µm, the so-called fingerprint region) and in the 2500-3300 cm^{-1} frequency range ($\lambda = 3$-4 µm, corresponding to the CH and OH bonds stretching region). The standard way to generate tunable ultrashort MIR pulses is by difference-frequency generation (DFG) between the signal and the idler pulses of a femtosecond optical parametric amplifier (OPA) [14], typically pumped with the fundamental wavelength (FW) of an amplified Ti:sapphire laser and spanning the 1.2-2.8 µm wavelength range [15]. The two collinearly generated signal and idler pulses are separated by a dichroic mirror, so that their relative delay can be adjusted, and then recombined using a second dichroic mirror. Several nonlinear crystals can be used, such as $AgGaS_2$ (AGS) and GaSe. The typical tuning range is in this case from 2.5 to 12 µm, allowing to cover all the vibrational frequencies of interest.

An alternative approach would be to generate the MIR pulses directly as the idler of an OPA, reducing the wavelength detuning between the pump and signal pulses to push the idler to longer wavelengths. This configuration is simpler as it eliminates one nonlinear optical process, the DFG step; however, it requires the fulfilment of two conditions: i) the availability of a nonlinear crystal with a broad transparency range in the MIR; ii) the possibility to pump this crystal with

#439298 https://doi.org/10.1364/OSAC.439298
Journal © 2021 Received 2 Aug 2021; revised 20 Oct 2021; accepted 20 Oct 2021; published 3 Nov 2021

OSA CONTINUUM

intense near-infrared (NIR) pulses without inducing two-photon absorption processes, which would degrade the performance of the OPA or even lead to crystal damage.

The most common nonlinear optical crystals, such as β-barium borate (BBO) or lithium triborate (LBO), are only transparent out to ≈3 μm. Other crystals, such as $LiIO_3$, $KNbO_3$, $KTiOPO_4$ (KTP) or its isomorphs, $MgO:LiNbO_3$, periodically poled lithium niobate (PPLN) and periodically poled stoichiometric lithium tantalate (PPSLT), display deeper MIR transparency out to 5 μm. Thanks to broadband phase matching conditions, they have been successfully exploited in simple OPA configurations for the generation of ultrashort pulses in the 3-4 μm wavelength range [16–19]. However, they do not allow to cover the vibrational fingerprint region, which is essential for spectroscopic applications and chemical resolution.

The majority of crystals with extended MIR transparency, such as $ZnGeP_2$ (ZGP), GaSe, $AgGaSe_2$ and $AgGaS_2$ (AGS) display an absorption edge in the visible (0.74 μm for ZGP, 0.65 μm for GaSe, 0.73 μm for $AgGaSe_2$ and 0.53 μm for AGS), thus suffering from two-photon absorption when directly pumped in the NIR by intense Ti:sapphire laser pulses. The situation improves when using Yb-based ultrafast lasers at 1.03 μm, as demonstrated by Heyne and coworkers who generated MIR pulses tunable from 3.5 to 9 μm using AGS [20]. An interesting recent alternative is $LiGaS_2$ (LGS) [21–24], which combines extended MIR transparency (out to 11.6 μm), a relatively large nonlinear optical coefficient (d_{eff} = 5-6 pm/V) and an absorption edge at 0.32 μm. The latter property allows direct pumping of an LGS-based OPA by an Yb laser [25,26]. In addition, when pumped at 1.03 μm, LGS satisfies a broadband phase matching condition in the 7.5-8.5 μm wavelength range, complementarily to the previously discussed class of crystals. Recently, Riedle and coworkers have generated from an LGS-based OPA broadband MIR pulses spanning 5-11 μm compressed to nearly transform-limited (TL) 32-fs duration, which is close to a single optical cycle at the carrier wavelength [27]. As a last approach to the generation of tunable MIR pulses, one should mention OPAs pumped at ≈2 μm by Ho- or Tm-based femtosecond laser systems [2,5,7,9,28]. In this case, the reduced quantum defect and the favorable phase-matching conditions enable the efficient generation of broadband MIR pulses. However, high power femtosecond lasers at 2 μm are still not very common and there are few commercial solutions available.

In this paper we present a simple OPA design, pumped by an amplified Yb:KGW laser, which directly generates broadly tunable MIR pulses, covering the whole vibrational spectrum from 3 to 10 μm. The two-stage architecture [29] starts with a first stage, pumped by the second harmonic (SH) of the Yb laser and employing a BBO crystal, which generates signal pulses tunable from 1.1 to 1.7 μm. The signal then seeds a second stage pumped by the FW of the laser that may employ either a PPLN crystal, to maximize the optical power in the 2.5-4.5 μm range, or a LGS crystal, to cover the full 3-10 μm region. This simple and easy to align source lends itself to a variety of ultrafast spectroscopy applications, such as time-resolved IR spectroscopy, 2D-IR spectroscopy and non-equilibrium studies of low-energy excitations in solids.

2. Setup scheme and phase matching conditions

Figure 1 shows the experimental setup of the two-stage OPA. The system is pumped by a regeneratively amplified femtosecond Yb:KGW laser (Pharos, Light Conversion), delivering 200-μJ, 220-fs pulses at 1.03 μm wavelength and 50 kHz repetition rate, corresponding to 10 W average power; for this experiment, only 2 W (40 μJ) were used. A 1.2 W fraction of this output is used to drive the first stage, which employs a non-collinear geometry and is pumped by the SH [29]. The 0.515-μm pump pulses with 3.65-μJ energy are produced by SH generation in a 3-mm-thick BBO crystal ($\theta = 23.4°$), while the seed pulses are obtained by white light continuum (WLC) generation in a 10-mm-thick YAG plate. The NIR part of the WLC is selected by a long-pass filter (LP1100, Thorlabs) and a non-collinear interaction angle of 5° is used to facilitate separation of the beams. Parametric amplification takes place in a 2-mm-thick BBO

OSA CONTINUUM

crystal cut for type I phase matching ($\theta = 23.4°$) and produces pulses with center wavelength tunable from 1.15 to 1.7 μm and energy variable from 35 to 175 nJ. The output pulses are rather broadband, with a bandwidth of around 25 THz, as they are generated from an OPA close to the degeneracy condition for type I phase matching [30]. These pulses act as a signal in a subsequent collinear OPA stage pumped by the remaining 0.8 W of the laser FW at 1.03 μm which produces high-power broadly tunable idler radiation over almost the entire MIR region.

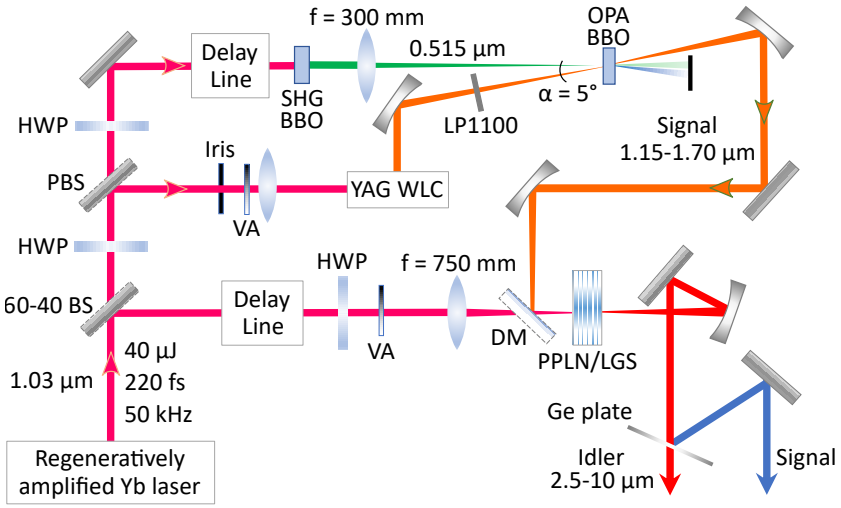

Fig. 1. Experimental setup of the OPA. HWP: half-wave plate; BS: beam splitter; PBS: polarizing beam splitter; VA: variable attenuator; DM: dichroic mirror.

The second stage of the OPA employs a strictly collinear geometry, to avoid angular dispersion of the idler pulses, and is directly pumped by the FW and seeded by the signal pulses from the first stage. For the 3-5 μm wavelength range, the most efficient option is a PPLN crystal with 1-mm length, 14-mm width, 1-mm thickness and a fan-out grating with poling period ranging from $\Lambda = 27.5$ μm to $\Lambda = 31.6$ μm (HC Photonics). This crystal allows to generate idler wavelengths from 2.06 μm to 4.34 μm. For an extended MIR tunability, we replace PPLN with a 2-mm-thick LGS crystal cut for type II phase matching ($\theta = 90°$, $\varphi = 38.4°$, Ascut Ltd), which returns a 20% larger nonlinearity than Type I. For both crystals, pump and signal beams are focused to diameters of ≈400 and ≈500 μm, respectively, so that it is easy to swap them, the only requirement being to rotate by 90° the pump polarization for LGS with a half-wave plate.

Figure 2 compares the properties of the OPA process in LGS and PPLN, in terms of phase-matching angles and group velocity mismatch (GVM) between the interacting pulses. In LGS, due to the small birefringence, the internal phase-matching angle varies significantly with the signal wavelength, implying an angular tilt over ~20° to fully exploit the available signal 1.15-1.7 μm tuning range, as shown in Fig. 2(a). In PPLN, over a smaller range from 1.35 to 1.7 μm due to the 5-μm transparency limit, the poling period for quasi-phase-matching needs adjustment from 27.5 to 30.5 μm, by simple sample translation in our case thanks to fan-out structure.

Figure 2(b) reports for the two crystals the GVM between the interacting pulses, defined as $\delta_{ij} = 1/v_{gi} - 1/v_{gj}$, where v_g is the group velocity and i,j correspond to the pump (p), signal (s) and idler (i) pulses. For LGS, the pump-signal GVM δ_{ps} remains exceptionally small (< 50 fs/mm) over the entire signal tuning range, setting favorable conditions for a large parametric gain. The pump-idler GVM δ_{pi} remains instead relatively high (200 fs/mm) and nearly constant over a large signal wavelength range, from 1.25 to 1.6 μm, while it drops to zero and changes sign at shorter wavelengths. This originates a relatively narrow conversion bandwidth over

OSA CONTINUUM

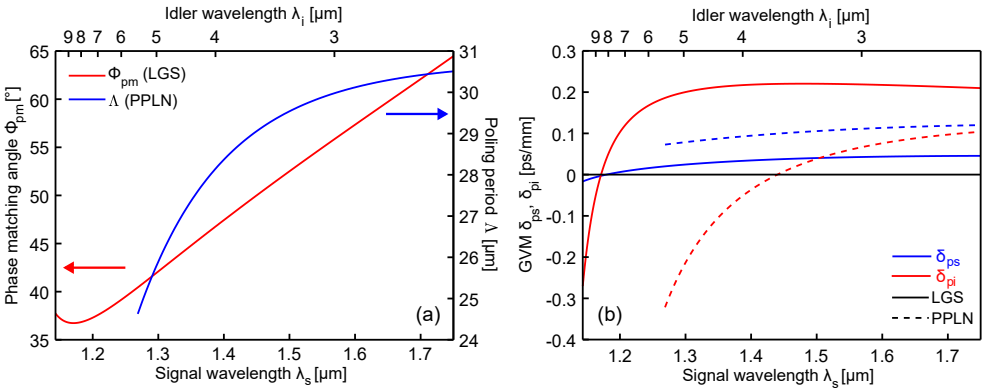

Fig. 2. a) Phase matching angle (λ_{pm}) and poling period (Λ) curves for LGS and PPLN pumped at $\lambda_p = 1.03\,\mu m$. b) Pump-signal (δ_{ps}, blue) and pump-idler (δ_{pi}, red) GVM curves for an LGS- (continuous lines) and a PPLN- (dashed lines) based collinear OPA pumped at $\lambda_p = 1.03\,\mu m$, as a function of the signal wavelength (λ_s).

most tuning range, combined with a much larger one around 1.17 μm (corresponding to an idler wavelength of 8.6 μm) where the two curves cross each other: at the crossing point signal and idler propagate with the same group velocity ($\delta_{si} = 0$) and this results in a broad gain bandwidth [31], as also evidenced by the corresponding stationary point in the phase-matching angle curve for LGS in Fig. 2(a). The GVM curves for PPLN show a more regular behavior, with a broader bandwidth due to a globally better matching between signal and idler group velocities, together with a favorable condition for high parametric gain below 1.35 μm, where signal and idler pulses have opposite velocities with respect to that of the pump pulses (different sign for δ_{ps} and δ_{pi}, as discussed in [31]). For PPLN the condition $\delta_{si} = 0$ is not reached in our tuning range, but the group velocities of signal and idler become very close around 1.7 μm, giving rise to a broader gain bandwidth.

3. Results and discussion

Figure 3 reports the signal (panel a) and idler (panel b) spectra at the output of the second OPA stage with LGS upon tuning the first stage wavelength and correspondingly adjusting the phase-matching angle. Overall, the spectra cover an extremely broad wavelength interval that combines a relatively large NIR range from 1.1 to 1.6 μm with an ultrabroad range in the MIR, from the high-energy vibrational region around 3 μm (3300 cm^{-1}) till the low-energy region at 10 μm and beyond (1000 cm^{-1}). As expected, the spectral width remains rather constant and relatively narrow (≈2.8 THz) over most part of the tuning range, except for the spectrum around 8.6 μm that benefits from the group velocity matching of signal and idler pulses. This spectrum, as well as its NIR counterpart, suffers from an evident hole induced by parasitic crystal absorption around 8 μm that is due to the specific LGS crystal adopted. Absorption peaks are also present in the spectra around 6-7 μm, in this case due to water vapor. The idler optical power, also shown in the figure, ranges from 8 to 28 mW, with the lowest power at longer wavelengths because of the larger quantum defect and of the higher crystal absorption. Considering the overall pump power of 2 W for the OPA, the conversion efficiency is good, although lower than what was achieved in previous works [32].

Figure 4(a) provides the signal amplification factor of the second stage calculated as a ratio between output and input signal power (blue trace): it varies from 5 to 11 upon increasing the signal wavelength, i.e. upon reducing the quantum defect of the idler. To better evaluate the frequency conversion capability of LGS we plot in Fig. 4(b) also an effective amplification factor

OSA CONTINUUM

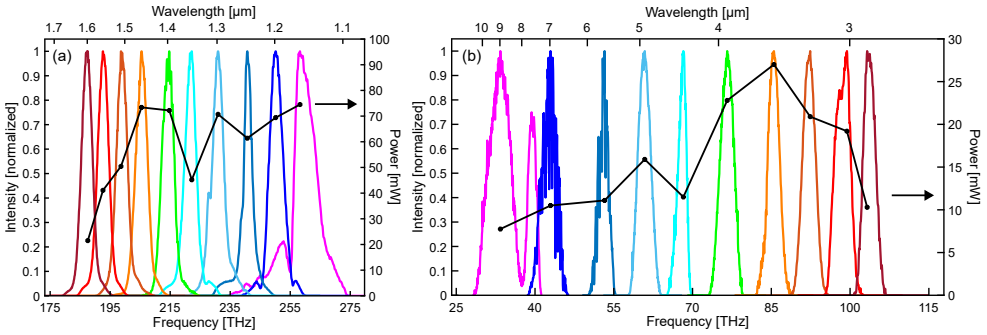

Fig. 3. Signal (a) and idler (b) spectra obtained from the second stage of the OPA using LGS, along with the associated average powers (black points with lines as guide to the eye). The same color has been used for each pair of corresponding signal and idler spectra.

(red), as obtained by rescaling the former values by the ratio between the input signal bandwidth, which is particularly large as it comes from the first broadband OPA stage, and the output signal bandwidth, which is reduced by the narrow phase-matching condition. With a spectral mismatch (highlighted in Fig. 4(b)) of about 4, the effective amplification is almost 4 times larger, with a peak around 40. This better accounts for the strong conversion efficiency of LGS and anticipates the possibility of generating higher idler powers by reducing the conversion bandwidth of the first stage. At the pump peak intensity of 50 GW/cm^2 here used, which is lower than the crystal damage threshold [33], the idler optical power was found stable within 0.85% rms.

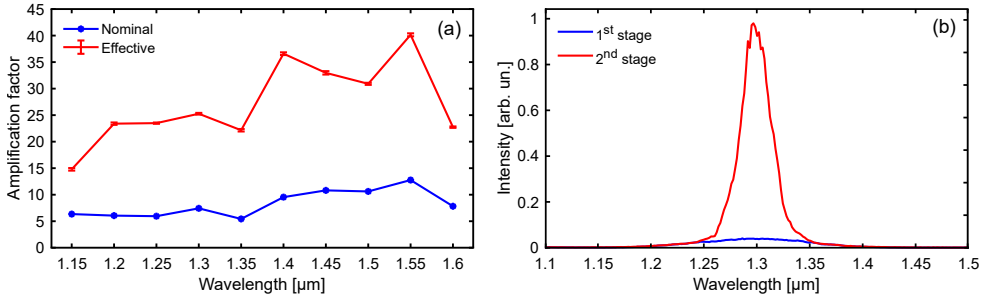

Fig. 4. a) Nominal and effective signal amplification factors for LGS as a function of signal wavelength. b) Comparison of first and second stage signal spectra for a representative wavelength.

Figure 5 reports the idler spectra and idler average powers obtained by replacing LGS with PPLN in the second OPA stage. The idler tuning range is here limited to below 5 μm because of the shorter wavelength absorption edge: as expected from the GVM diagrams of Fig. 2(b) and also thanks to a crystal thickness of only 1 mm, the bandwidth of the pulses is comparatively larger than for LGS and reaches a peak of 9.75 THz at an idler wavelength of 2.8 μm, that is closer to degenerate interaction conditions. Thanks to a three times larger second order nonlinear coefficient, PPLN offers at the same wavelength a 3-fold higher power than LGS, despite the use of a lower pump power (0.65 W) because of a lower optical damage threshold. In terms of duration, pulses from LGS are easily predicted to be very close to their TL values in the 3-7 μm range: in fact, with a crystal GDD (Group-Delay-Dispersion) lower than -1500 fs^2/mm, no appreciable broadening occurs over a 2-mm-thick crystal for pulses with a TL duration of 150-250 fs. Conversely, at 8.6 μm, where the TL is 77 fs and the GDD amounts to -4050 fs^2/mm, simulations predict a 300 fs pulse duration, thus quite far away from the TL but still of the same

OSA CONTINUUM

order of magnitude of the pulse durations at wavelengths < 7 µm. In a pump-probe spectroscopy arrangement and without chirp compensation we thus expect a time resolution of about 300 fs. For PPLN, which displays broader bandwidths corresponding to TL durations of 50-140 fs, simple temporal compression schemes using dispersive plates have been already shown suitable for nearly single-cycle pulse synthesis, thanks to the availability of several positive dispersion (e.g., ZnSe) and negative dispersion (e.g., CaF_2) materials in the 2.5-5 µm region [34].

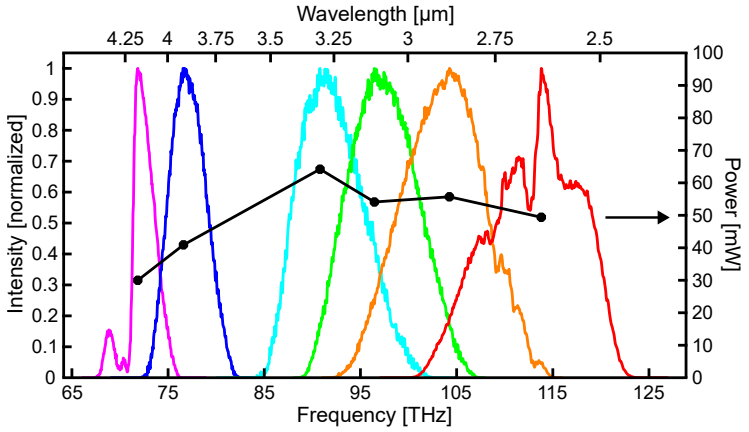

Fig. 5. Idler spectra generated by the second OPA stage with PPLN, along with the corresponding output power (black points with line as guide to the eye). The dip around 4.3 µm is due to CO_2 absorption.

4. Conclusions

In conclusion, our two-stage OPA configuration is a versatile setup for the generation of femtosecond pulses over a broad range of wavelengths in the MIR, covering both the fingerprint and the CH/OH vibrational windows, for a wide variety of time-resolved spectroscopy studies. The avoidance of the traditional DFG stage to access the MIR range simplifies the setup while enabling high conversion efficiencies. Of the two crystals employed in the second stage, PPLN is more suitable for the generation of broadband pulses in the CH/OH stretching range, while LGS allows extending the tunability to the fingerprint region. Thanks to the outstanding power scaling capability of Yb technology and to the chance to improve the amplification efficiency by a better matching of the conversion bandwidths of the two OPA stages, this configuration may also be of interest for ultra-high brightness MIR light generation with a table-top device, for applications such as Fourier-transform IR [35] and photothermal IR [36] microscopy.

Funding. European Research Council (816313); Regione Lombardia (sPATIALS3, POR FESR 2014-2020 - Call HUB).

Disclosures. The authors declare no conflicts of interest.

Data availability. Data presented in this paper are not publicly available but may be obtained from the authors upon request.

References

1. T. Popmintchev, M.-C. Chen, D. Popmintchev, P. Arpin, S. Brown, S. Ališauskas, G. Andriukaitis, T. Balčiunas, O. D. Mücke, A. Pugzlys, A. Baltuška, B. Shim, S. E. Schrauth, A. Gaeta, C. Hernández-García, L. Plaja, A. Becker, A. Jaron-Becker, M. M. Murnane, and H. C. Kapteyn, "Bright coherent ultrahigh harmonics in the keV regime from mid-infrared femtosecond lasers," Science **336**(6086), 1287–1291 (2012).
2. L. von Grafenstein, M. Bock, D. Ueberschaer, E. Escoto, A. Koç, K. Zawilski, P. Schunemann, U. Griebner, and T. Elsaesser, "Multi-millijoule, few-cycle 5 µm OPCPA at 1 kHz repetition rate," Opt. Lett. **45**(21), 5998–6001 (2020).

OSA CONTINUUM

3. G. Ycas, F. R. Giorgetta, E. Baumann, I. Coddington, D. Herman, S. A. Diddams, and N. R. Newbury, "High-coherence mid-infrared dual comb spectroscopy spanning 2.6 to 5.2 µm," Nat. Photonics **12**(4), 202–208 (2018).
4. A. V. Muraviev, V. O. Smolski, Z. E. Loparo, and K. L. Vodopyanov, "Massively parallel sensing of trace molecules and their isotopologues with broadband subharmonic mid-infrared frequency combs," Nat. Photonics **12**(4), 209–214 (2018).
5. D. Sanchez, M. Hemmer, M. Baudisch, S. L. Cousin, K. Zawilski, P. Schunemann, O. Chalus, C. Simon-Boisson, and J. Biegert, "7 µm, ultrafast, sub-millijoule-level mid-infrared optical parametric chirped pulse amplifier pumped at 2 µm," Optica **3**(2), 147–150 (2016).
6. L. Maidment, O. Kara, P. G. Schunemann, J. Piper, K. McEwan, and D. T. Reid, "Long-wave infrared generation from femtosecond and picosecond optical parametric oscillators based on orientation-patterned gallium phosphide," Appl. Phys. B **124**(7), 143 (2018).
7. T. P. Butler, N. Lilienfein, J. Xu, N. Nagl, C. Hofer, D. Gerz, K. F. Mak, C. Gaida, T. Heuermann, M. Gebhardt, J. Limpert, F. Krausz, and I. Pupeza, "Multi-octave spanning, Watt-level ultrafast mid-infrared source," JPhys Photonics **1**(4), 044006 (2019).
8. M. Seidel, X. Xiao, S. A. Hussain, G. Arisholm, A. Hartung, K. T. Zawilski, P. G. Schunemann, F. Habel, M. Trubetskov, V. Pervak, O. Pronin, and F. Krausz, "Multi-watt, multi-octave, mid-infrared femtosecond source," Sci. Adv. **4**(4), 4 (2018).
9. C. Gaida, M. Gebhardt, T. Heuermann, F. Stutzki, C. Jauregui, J. Antonio-Lopez, A. Schülzgen, R. Amezcua-Correa, A. Tünnermann, I. Pupeza, and J. Limpert, "Watt-scale super-octave mid-infrared intrapulse difference frequency generation," Light: Sci. Appl. **7**(1), 94 (2018).
10. M.D. Fayer (ed.), *Ultrafast Infrared Vibrational Spectroscopy* (Taylor and Francis, 2013).
11. P. Hamm and M.T. Zanni, *Concepts and Methods of 2d Infrared Spectroscopy* (Cambridge University, 2011).
12. C. Poellmann, P. Steinleitner, U. Leiersede, P. Nagler, G. Plechinger, M. Porer, R. Bratschitsch, C. Schüller, T. Korn, and R. Huber, "Resonant internal quantum transitions and femtosecond radiative decay of excitons in monolayer WSe2," Nat. Mater. **14**(9), 889–893 (2015).
13. M. Först, R. Mankowsky, and A. Cavalleri, "Mode-Selective Control of the Crystal Lattice," Acc. Chem. Res. **48**(2), 380–387 (2015).
14. F. Seifert, V. Petrov, and M. Woerner, "Solid-state laser system for the generation of midinfrared femtosecond pulses tunable from 3.3 to 10 µm," Opt. Lett. **19**(23), 2009–2011 (1994).
15. R. A. Kaindl, M. Wurm, K. Reimann, P. Hamm, A. M. Weiner, and M. Woerner, "Generation, shaping, and characterization of intense femtosecond pulses tunable from 3 to 20 µm," J. Opt. Soc. Am. B **17**(12), 2086–2094 (2000).
16. A. Boulesbaa, O. Isaienko, A. Tuladhar, and E. Borguet, "Generation of sub-30-fs microjoule mid-infrared pulses for ultrafast vibrational dynamics at solid/liquid interfaces," Opt. Lett. **38**(23), 5008–5011 (2013).
17. D. Brida, M. Marangoni, C. Manzoni, S. De Silvestri, and G. Cerullo, "Two-optical-cycle pulses in the mid-infrared from an optical parametric amplifier," Opt. Lett. **33**(24), 2901–2903 (2008).
18. O. Chalus, P. K. Bates, M. Smolarski, and J. Biegert, "Mid-IR short-pulse OPCPA with micro-Joule energy at 100kHz," Opt. Express **17**(5), 3587–3594 (2009).
19. C. Heese, C. R. Phillips, L. Gallmann, M. M. Fejer, and U. Keller, "Ultrabroadband, highly flexible amplifier for ultrashort midinfrared laser pulses based on aperiodically poled Mg:$LiNbO_3$," Opt. Lett. **35**(14), 2340–2342 (2010).
20. V. Kozich, A. Moguilevski, and K. Heyne, "High energy femtosecond OPA pumped by 1030 nm Yb:KGW laser," Opt. Commun. **285**(21-22), 4515–4518 (2012).
21. K. Kato, K. Miyata, L. Isaenko, S. Lobanov, V. Vedenyapin, and V. Petrov, "Phase-matching properties of $LiGaS_2$ in the 1.025-10.910 µm spectral range," Opt. Lett. **42**(21), 4363–4366 (2017).
22. B. H. Chen, T. Nagy, and P. Baum, "Efficient middle-infrared generation in $LiGaS_2$ by simultaneous spectral broadening and difference-frequency generation," Opt. Lett. **43**(12), 2876 (2018).
23. M. Knorr, J. Raab, M. Tauer, P. Merkl, D. Peller, E. Wittmann, E. Riedle, C. Lange, and R. Huber, "Phase-locked multi-terahertz electric fields exceeding 13 MV/cm at a 190 kHz repetition rate," Opt. Lett. **42**(21), 4367–4370 (2017).
24. Z. Heiner, L. Wang, V. Petrov, and M. Mero, "Broadband vibrational sum-frequency generation spectrometer at 100 kHz in the 950-1750cm−1 spectral range utilizing a $LiGaS_2$ optical parametric amplifier," Opt. Express **27**(11), 15289–15297 (2019).
25. S. B. Penwell, L. Whaley-Mayda, and A. Tomakoff, "Single stage MHz mid-IR OPA using $LiGaS_2$ and a fiber laser pump source," Opt. Lett. **43**(6), 1363–1366 (2018).
26. S. Qu, H. Liang, K. Liu, X. Zou, W. Li, Q. J. Wang, and Y. Zhang, "9 µm few-cycle optical parametric chirped-pulse amplifier based on $LiGaS_2$," Opt. Lett. **44**(10), 2422–2425 (2019).
27. B.-H. Chen, E. Wittmann, Y. Morimoto, P. Baum, and E. Riedle, "Octave-spanning single-cycle middle-infrared generation through optical parametric amplification in $LiGaS_2$," Opt. Express **27**(15), 21306–21318 (2019).
28. T. Kanai, P. Malevich, S. S. Kangaparambil, K. Ishida, M. Mizui, K. Yamanouchi, H. Hoogland, R. Holzwarth, A. Pugzlys, and A. Baltuska, "Parametric amplification of 100 fs mid-infrared pulses in ZnGeP2 driven by a Ho:YAG chirped-pulse amplifier," Opt. Lett. **42**(4), 683–686 (2017).
29. M. Bradler, C. Homann, and E. Riedle, "Mid-IR femtosecond pulse generation on the microjoule level up to 5 µm at high repetition rates," Opt. Lett. **36**(21), 4212–4214 (2011).

OSA CONTINUUM

30. D. Brida, C. Manzoni, G. Cirmi, M. Marangoni, S. Bonora, P. Villoresi, S. De Silvestri, and G. Cerullo, "Few-optical-cycle pulses tunable from the visible to the mid-infrared by optical parametric amplifiers," J. Opt. **12**(1), 013001 (2010).
31. G. Cerullo and S. De Silvestri, "Ultrafast optical parametric amplifiers," Rev. Sci. Instrum. **74**(1), 1–18 (2003).
32. Z. Heiner, V. Petrov, and M. Mero, "Efficient, sub-4-cycle, 1-μm-pumped optical parametric amplifier at 10 μm based on $BaGa_4S_7$," Opt. Lett. **45**(20), 5692–5695 (2020).
33. I. Pupeza, D. Sánchez, J. Zhang, N. Lilienfein, M. Seidel, N. Karpowicz, T. Paasch-Colberg, I. Znakovskaya, M. Pescher, W. Schweinberger, V. Pervak, E. Fill, O. Pronin, Z. Wei, F. Krausz, A. Apolonski, and J. Biegert, "High-power sub-two-cycle mid-infrared pulses at 100 MHz repetition rate," Nat. Photonics **9**(11), 721–724 (2015).
34. N. Bigler, J. Pupeikis, S. Hrisafov, L. Gallmann, C. R. Phillips, and U. Keller, "High-power OPCPA generating 1.7 cycle pulses at 2.5 μm," Opt. Express **26**(20), 26750–26757 (2018).
35. S. Mittal, K. L. S. Yeh Leslie, S. Kenkel, A. Kajdacsy-Balla, and R. Bhargava, "Simultaneous cancer and tumor microenvironment subtyping using confocal infrared microscopy for all-digital molecular histopathology," Proc. Natl. Acad. Sci. U. S. A. **115**(25), E5651–E5660 (2018).
36. M. Tamamitsu, K. Toda, H. Shimada, T. Honda, M. Takarada, K. Okabe, Y. Nagashima, R. Horisaki, and T. Ideguchi, "Label-free biochemical quantitative phase imaging with mid-infrared photothermal effect," Optica **7**(4), 359–366 (2020).